Effect of strain on the stacking fault energy of copper: A first-principles study

P. S. Branicio,[1,*] J. Y. Zhang,[1] and D. J. Srolovitz[2]

[1]*Institute of High Performance Computing, Agency for Science, Technology and Research, 1 Fusionopolis Way, 16-16 Connexis 138632, Singapore*

[2]*Department of Materials Science and Engineering and Department of Mechanical Engineering and Applied Mechanics, University of Pennsylvania, 3231 Walnut Street, Philadelphia, Pennsylvania 19104, USA*

(Received 24 December 2012; revised manuscript received 11 June 2013; published 26 August 2013)

The intrinsic stacking fault energy (SFE) of copper under volumetric, longitudinal, and shear strains is investigated using density functional theory (GGA-PBE). Calculations are performed using a copper slab model aligned perpendicular to the (111) intrinsic stacking fault plane. The calculated SFE for unstrained copper is $\gamma = 41$ mJ/m^2. Results show a strong dependence of γ on strain and distinct behavior for different types of strain: (a) volumetric and longitudinal in the direction perpendicular to the stacking fault, (b) longitudinal parallel to the stacking fault, and (c) shear parallel to the stacking fault. In the first case (a), the SFE decreases monotonically with strain with a slope $d\gamma/d\varepsilon|_{\varepsilon=0} = -0.44$ J/m^2 and -0.87 J/m^2 for volumetric and longitudinal, respectively, and with $d^2\gamma/d\varepsilon^2 > 0$. In contrast, for longitudinal strain parallel to the stacking fault (b), the SFE dependence exhibits $d^2\gamma/d\varepsilon^2 < 0$ with a maximum at $\varepsilon \approx -0.015$. For the case of shear parallel to the stacking fault (c), the SFE is nearly constant at small and moderately large strain, but drops rapidly at very large strain (by a factor of 1/3 for $\langle\bar{1}10\rangle\{111\}$ shear at $\varepsilon = \pm 0.1$). For large $\langle 11\bar{2}\rangle\{111\}$ shear strains, the SFE can either increase or decrease at large strain depending on the sign of the strain. In volumetric or longitudinal (perpendicular to the stacking fault) tension and longitudinal strain in the boundary plane (and for some shear directions), the SFE can become negative, implying a limit on the stability of the fcc crystal structure. The strong dependence of the SFE on strain suggests deep implications for the mechanical properties, microstructural evolution, and dynamic plasticity of metals at high pressure, during severe plastic deformation, and in shock-loading conditions.

DOI: 10.1103/PhysRevB.88.064104 PACS number(s): 61.72.Nn, 62.20.F−, 71.15.Mb

I. INTRODUCTION

Intrinsic stacking faults play a very important role in determining deformation mechanism and mechanical properties in face-centered-cubic (fcc) metals.[1–6] The stacking fault energy (SFE) determines equilibrium partial dislocation separations, the tendency towards dislocation cross slip, the propensity of twinning, etc. In the perfect fcc crystal lattice, three equivalent close-packed planes (referred to here as A, B, and C) are aligned along $\langle 111\rangle$ directions following a stacking sequence $ABCABCABC\ldots$. An intrinsic stacking fault occurs when the stacking sequence is altered by removal of one of the planes in this stacking sequence, e.g., $ABCABABC\ldots$. The SFE is the difference in energy between the crystal with a stacking fault and a crystal with a perfect stacking sequence, normalized by the stacking fault area. The SFE can be calculated using atomistic models following exactly this definition. Experimentally, the SFE is usually determined indirectly by measuring the separation between Shockley partial dislocations.[7–9] This partial dislocation separation results from a balance between the elastic repulsion between the partial dislocations and the attraction generated by the energy penalty associated with the energy of the stacking fault, as first proposed by Heidenreich and Shockley.[10] Following the theory of Heidenreich and Shockley, Fullman[11] deduced the value of the SFE for Cu to be 42 mJ/m^2. This initial measurement was followed by many other investigations of the SFE in fcc metals using a variety of methods, often reporting a wide range of values (e.g., see the review by Gallagher).[7]

One of the most important effects of the SFE is its role in determining the partial dislocation separation. Dislocations have more difficulty to cross slip and climb when the partial separation is large (SFE is low).[12] One example of the impact of SFE on cross slip may be seen during severe plastic deformation (SPD) processing[13] of fcc Cu-Al alloys; the SPD steady-state grain size decreases with increasing stacking fault energy (decreasing partial separation), presumably because the SFE determines the probability of cross slip.[14–16] Experimental results suggest that the ductility and strength of Cu-Al alloys can be simultaneously improved by decreasing their SFE. The widely known effects of SFE on the mechanical behavior of metals and alloys indicates the importance of determining the stacking fault energy, the ability to manipulate it via alloying, and understanding its dependence on external parameters such as temperature and strain. The latter is the focus of this investigation.

First-principles methods such as the density functional theory (DFT) offer a suitable approach to directly determine the SFE. However, accurate determination of the SFE by DFT is computationally challenging, since it involves the use of large supercells and stringent convergence criteria to properly calculate the minute differences in system energy introduced by the presence of a stacking fault. There are two major procedures for the calculation of the SFE using DFT. One can use periodic systems[17] or crystal slabs.[18] The use of periodic systems has the advantages of not requiring knowledge of a corresponding perfect crystalline reference system and avoidance of the complicating presence of free surfaces. It also allows the study of temperature effects. However, by using periodic systems, one has to consider a set of at least three stacking faults and make use of very large supercells to ensure proper convergence. On the other hand, the use of crystal slabs requires a reference system,

to eliminate the effect of surfaces. Nevertheless, it allows relatively smaller supercells. Due to these challenges and differences in first-principles methodologies a wide range of theoretical SFE values[19–24] have been reported in the literature for copper with varying degrees of agreement with experimentally reported data.[8,11,25,26]

The SFE is commonly considered to be an intrinsic constant material property. However, it is known that its value can vary with temperature and strain. In the face of this and the importance of the SFE for understanding the mechanical properties of fcc metals it is surprising that there are few reports on the temperature and strain dependence of the SFE.[18,22]

The dependence of the SFE on temperature is expected to be mild.[17] However, recent reports claim significant strain effects on the SFE.[18,22] Using empirical modeling, Henio *et al.*[22] showed that the SFE of copper can undergo significant change with strain, both for longitudinal strain in the ⟨111⟩ direction as well as for volumetric strain. However, limitations of empirical modeling based on the embedded atom model (EAM) potential restrict the investigation to moderate strains. Brandl *et al.*[18] investigated the role of volumetric and shear strain fields on the generalized SFE in Al, Cu, and Ni and the ratio of the stable to unstable stacking fault energies using a first-principles method. They reported significant changes in the SFE of these fcc metals even under mild strain ($\varepsilon = 0.02$). Such strain effects can be of particular importance for the mechanical behavior of fcc metals in both shock-loading conditions and in the deformation of nanomaterials.

In this work, we focus on the accurate determination of the SFE of copper under a wide range of loading conditions using DFT. In particular, we consider the effects of volumetric (hydrostatic), uniaxial, and shear strains (in multiple independent directions). To calculate quantities relevant for high pressure and shock conditions we evaluate the dependence of the SFE under strains as large as $\varepsilon = 0.1$. The results show a very strong dependence of the SFE on strain and significant effects under some types of strain even for small elastic deformation.

II. COMPUTATIONAL DETAILS

The present study employs the projector augmented wave (PAW) method[27] within the generalized gradient approximation plane wave using the DFT code VASP.[28] We adopt the Perdew, Burke and Ernzerhof (PBE)[29] version of the exchange correlation energy functional and the Methfessel and Paxton method[30] to smear the Fermi surface. Within the PAW method the experimental equation of state for Cu was shown to be accurately reproduced up to 100 GPa.[31] The cutoff energy, k-mesh grid, and the number of fcc atomic layers used along the [111] direction are carefully tested for convergence with respect to system energy, lattice parameters, and the SFE itself. Details of the convergence test can be found in the Appendix. Here, we use a 500 eV cutoff energy, 24 × 24 × 1 (290 irreducible k points) k-mesh grid following the Monkhorst-Pack method,[32] and 24 fcc atomic layers along the ⟨111⟩ direction. The energy difference between subsequent self-consistent field iterations is less than 10^{-6} eV/cell for the electronic ground state. For instance, the lattice constant of copper is calculated to be 3.637 Å (after letting the atomic positions and the simulation box fully relax), which is in excellent agreement with the experimental value 3.613 Å measured via x-ray diffraction.[33]

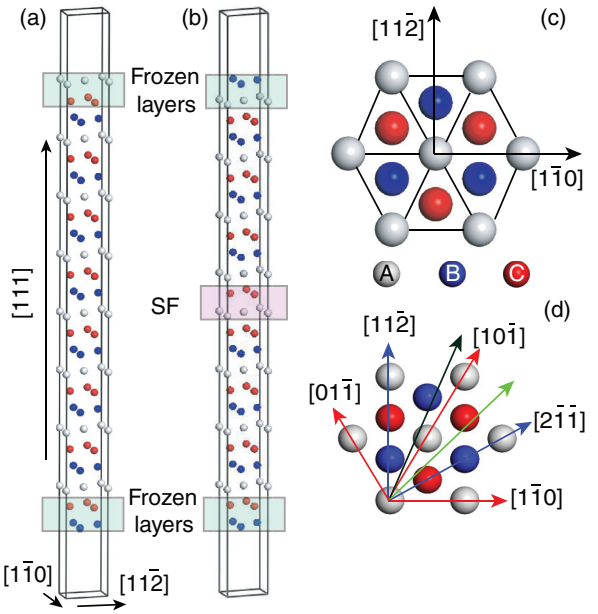

FIG. 1. (Color online) Illustration of the atomic structures and computational cell used in the SFE calculations. (a) Copper fcc slab with 24 (111) layers along the [111] direction used as a reference. (b) Copper fcc slab with a single stacking fault, highlighted by the pink rectangle. In both structures, the bottom and top two layers (highlighted by the light blue rectangles) are frozen and a 15 Å vacuum layer separates the periodic images in the supercell. (c) Illustration of the Cu fcc atomic layers on three sequential (111) planes (shown in three colors). (d) Schematic description of the directions in the (111) plane along which uniaxial strains are applied. Equivalent directions are shown in same colors. The two directions with irrational Miller index (shown in green and black) make angles of $\pi/4$ and $3\pi/8$ with respect to the [1$\bar{1}$0] direction, respectively.

A schematic illustration of the simulation cell is shown in Fig. 1. We construct supercells with 24 closed-packed (111) atomic layers along the [111] direction with and without a stacking fault. A separation layer of 15 Å vacuum is imposed at the top and bottom of the supercell to avoid interaction between the periodic images. Figure 1(d) shows the different directions along which we apply uniaxial strains within the (111) plane. The strains are produced by suitably rescaling the zero-strain supercell structure, with relaxed atomic positions and cell size, by a factor of $(1 + \varepsilon)$, where ε is the magnitude of the strain. Very large strains, up to $\varepsilon = 0.1$, are employed to investigate the value of SFE in highly strained environments such as those present in high pressure and shock-loading conditions. For reference, we investigate the three different approaches of loading in the [111] direction: (1) simple strain (i.e., pure uniaxial strain), (2) volume-conserving strain (i.e., apply strain ε in the [111] direction and strains $-\varepsilon/2$ in two orthogonal directions such that the volume is conserved), and (3) a strain consistent with uniaxial tension (i.e., apply strain ε in the [111] direction and strains $-\nu\varepsilon$ in two orthogonal directions, where ν is the Poisson's ratio). For loading in directions other than [111] we employ only simple strain.

TABLE I. Comparison of stacking fault energy in units of (mJ/m^2) with other experimental and theoretical reports.

Method	Publication/year	SFE (mJ/m^2)
Theor.[a]	This work, 2013	41
Theor.[b]	Cotteril *et al*. (Ref. 19), 1966	30
Theor.[c]	Schweizer *et al*. (Ref. 20), 1992	50
Theor.[d]	Rosengaard *et al*. (Ref. 21), 1993	56
Theor.[e]	Henio *et al*. (Ref. 22), 1999	78
Theor.[f]	Ogata *et al*. (Ref. 23), 2002	39
Theor.[g]	Qi *et al*. (Ref. 24), 2007	33
Expt.[h]	Fullman (Ref. 11), 1951	42
Expt.[i]	Howie *et al*. (Ref. 8), 1961	40
Expt.[j]	Peissker (Ref. 25), 1965	50
Expt.[k]	Stobbs *et al*. (Ref. 26), 1971	41

[a]DFT-GGA-PBE.
[b]Reference 19: Morse potential.
[c]Reference 20: DFT-LDA.
[d]Reference 21: Tight binding linear muffin tin orbital Green's function.
[e]Reference 22: EMT/EAM potential.
[f]Reference 23: DFT-GGA-PW91.
[g]Reference 24: DFT-GGA-PW91.
[h]Reference 11: Measurements of intersections of grain boundaries and coherent twins boundaries.
[i]Reference 8: Measurements of radius of curvature of extended dislocations by TEM.
[j]Reference 25: Measurements of dependence of critical stress for cross slip with strain rate.
[k]Reference 26: Measurement of partial dislocations spacing.

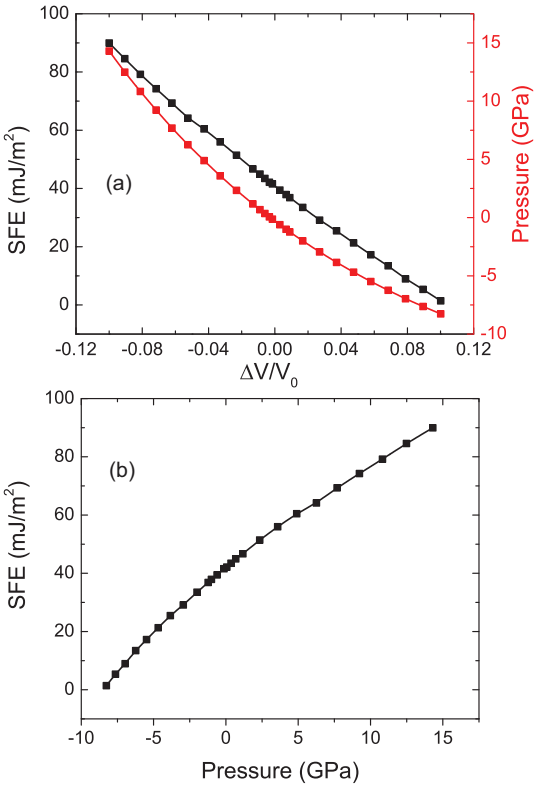

FIG. 2. (Color online) SFE as a function of volumetric strain (a) and pressure (b). In (a) the pressure, in red, is also shown as a function of volumetric strain for reference.

III. SFE OF UNSTRAINED COPPER

We first determine the SFE of unstrained copper both to serve as a baseline and to determine the nature of the agreement between our results and previous published values. Table I shows our calculated value of the SFE for copper as well as values reported in the literature using experimental[8,11,25,26,34] and theoretical[19–24] methods. Experimental SFE values vary widely, possibly due to different experimental conditions, measuring methods, sample purity, and assumptions in the analyses. The theoretical values show even a wider range of SFE values, owing to different calculation methods, approximations, interatomic potentials, convergence criteria, etc. Therefore, comparison with the literature is not a straightforward task and is of only limited utility. Our calculated SFE value for copper is 41 mJ/m^2. This is very close to the preponderance of experimental results and near the center of the range of values reported from theoretical studies.

IV. SFE OF COPPER UNDER VOLUMETRIC STRAIN ($\Delta V/V$)

It is important to understand the behavior of the SFE under volumetric (hydrostatic) strain in order to analyze the deformation behavior at high pressure and under shock-loading conditions. Figure 2(a) shows the SFE as a function of isotropic expansion and compression over a wide range of elastic strain $-0.1 \leqslant (\varepsilon = \Delta V/V) \leqslant 0.1$. This figure also shows the corresponding pressure versus strain. At small strains, the SFE is proportional to the volumetric strain with a slope of $d\gamma/d\varepsilon|_{\varepsilon=0} = -0.44$ J/m^2. The value of the SFE decreases monotonically with increasing volumetric strain. In the large strain range applied, the SFE remains positive, though it is close to zero at $\varepsilon = 0.1$. A negative SFE suggests loss of stability of the fcc lattice structure, which could be achieved at strains larger than 0.1. The dependence of the SFE on the strain can be well described by a cubic polynomial fit of the form $\gamma(\mathrm{J/m^2}) = A + B\varepsilon + C\varepsilon^2 + D\varepsilon^3$. Coefficients of the fitting are provided in Table II. The parametric dependence of the SFE with pressure, shown in Fig. 2(b), is also well described by a cubic polynomial fit (please see coefficients in Table II). The calculated SFE under isotropic (hydrostatic) strain is in striking contrast with the prediction of a previous calculation performed using an EAM potential for copper.[22] In that work, the reported SFE as a function of strain in the range $-0.02 < \varepsilon < 0.02$ shows a parabolic dependence with maximum near $\varepsilon = 0$ and decreases with increasing strain. The calculated SFE as a function of longitudinal strain in the [111] direction (discussed below) is also in striking contrast with our first-principles results—this suggests that the predicted SFE energies for strained systems calculated with EAM potentials should be used with extreme caution.

TABLE II. Coefficients in the fitted third order polynomial curves of the SFE as a function of volumetric strain, strain along [111] direction, and along directions in the (111) plane. SFE unit is J/m^2 except for the SFE(P), which is mJ/m^2, for pressure given in GPa. The critical strains (CS) where the SFE becomes negative are also shown if present.

	A	*B*	*C*	*D*	CS1	CS2
			Volumetric strain			
SFE (ε)	0.04	−0.43	0.47	− 1.16		
SFE (P)	42.12	4.04	− 0.08	0.003		
			Strain in the [111] direction			
Simple strain	0.04	− 0.91	3.24	− 9.73	0.05	
Uniaxial stress	0.04	− 0.80	1.40	1.18	0.06	
Volume conserving	0.04	− 0.69	1.14	− 2.26	0.06	
			Strain in the (111) plane			
$[1\bar{1}0]$	0.04	− 0.22	− 6.72	7.64	− 0.09	0.07
$3\pi/8$ to $[1\bar{1}0]$	0.04	− 0.22	− 6.39	10.86	− 0.09	0.07
$[2\bar{1}\bar{1}]$	0.04	− 0.24	− 7.89	49.97	− 0.07	0.08
$\pi/4$ to $[1\bar{1}0]$	0.04	− 0.26	− 6.89	32.35	− 0.08	0.07

V. SFE OF COPPER UNDER UNIAXIAL STRAIN PARALLEL AND PERPENDICULAR TO [111]

Since Cu, like all crystalline materials, is anisotropic, it is interesting to investigate the variation of the SFE as a function of strain in different directions. Since the (111) plane is the preferred glide plane for edge dislocations in fcc metals[34] it is interesting to examine how the SFE varies with uniaxial strain applied both in this plane and perpendicular to it.

For longitudinal strain applied along the [111] direction (perpendicular to the stacking fault plane), we calculate the SFE values following three procedures: (i) simple strain (pure uniaxial strain, non-volume-conserving), (ii) volume conserving, and (iii) uniaxial stress. For the simple strain, case (i), we simply rescale the cell dimension in the [111] direction (z direction) by $(1 + \varepsilon)$, while keeping the other two cell dimensions (x and y) fixed. In the volume-conserving procedure, case (ii), we apply the desired strain along the [111] direction, by scaling the length of the computational cell by $(1 + \varepsilon)$ in the z direction, while rescaling the cell dimensions along the x and y directions by $(1 + \varepsilon)^{-1/2}$, in order to keep the volume constant. This is consistent with a Poisson's ratio of exactly $1/2$ in the linear elastic limit. For the uniaxial stress case (iii), we changed the length of the unit cell in the [111] direction by $(1 + \varepsilon)$ and rescale the cell dimensions along the x and y directions to enforce zero stress in these directions. In the linear elastic limit, this implies that we allow the system to deform in a manner consistent with its own Poisson's ratio—giving a volume change between that of the other two cases.

The last procedure is typical of an engineering tensile test, where the Poisson's ratio of the material defines the perpendicular strain of the sample. In the present calculations, this requires a zero lateral stress optimization of the supercell and will give a result that is simulation cell size dependent. The surface (and interfaces) stress will generate a residual stress in the system which will depend on the length of the sample along the [111] direction. The residual stress decreases gradually with increasing cell length. However, for any supercell that can be practically treated using our first-principles approach, the residual stress will interfere with the supercell optimization and affect the value of the calculated SFE. Therefore, in our implementation, we determined the appropriate Poisson's ratio as a function of strain and applied it during the deformation rather than optimizing a very large supercell. Fortunately, the Poisson's ratio can be calculated reliably through optimization of the geometry of a fully periodic copper unit cell under strain along the [111] direction. Figure 3 shows the calculated dependence of the Poisson's ratio on longitudinal strain along the [111] direction. The value of the Poisson's ratio, calculated from the anisotropic elastic constants[35–37] is in good agreement with the present results. For reference, we also added the Poisson's ratio for polycrystalline Cu (Ref. 38) 0.34 to Fig. 3—the discrepancy is simply related to the anisotropy of Cu.[39] The analytical calculation of the Poisson's ratio as a function of strain in terms of the second, third, and higher order elastic constants is in theory possible but this is not the focus of the present work and is not included here.[40] Figure 3 shows that the Poisson's ratio of copper, commonly assumed to be constant, varies from 0.42 to 0.19 within the applied strain range considered here, $-0.1 < \varepsilon < 0.1$.

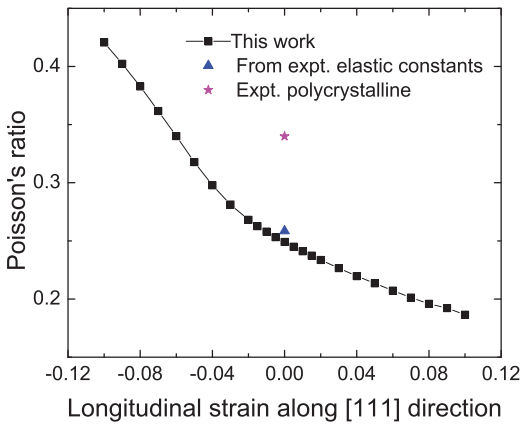

FIG. 3. (Color online) Poisson's ratio as a function of the longitudinal strain along the [111] direction. The line is a guide for the eyes. The Poisson's ratio derived from the experimental, anisotropic elastic constants[36] is shown for comparison together with the experimental Poisson's ratio for polycrystalline Cu.[38]

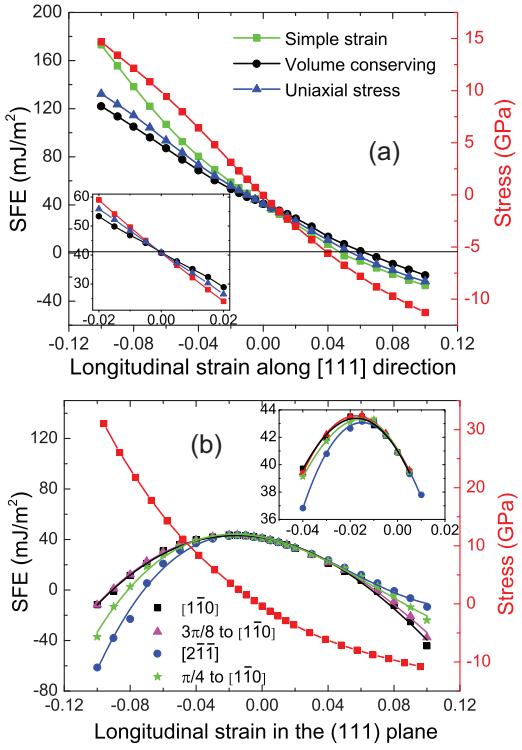

FIG. 4. (Color online) SFE versus uniaxial strain in the direction perpendicular (a) to the stacking fault and (b) in the plane of the stacking fault. (a) SFE as a function of the longitudinal strain perpendicular to the (111) stacking fault for cases of simple (uniaxial) strain, uniaxial stress, and where the volume is conserved. The induced stress for the uniaxial stress case is shown in red. (b) SFE as a function of longitudinal strain along different directions in the (111) stacking fault plane as illustrated in Fig. 1(d). The curves in (b) show third order polynomial fittings. The inset shows the behavior of the SFE with strain at small strain. The induced stress for longitudinal strain along [1$\bar{1}$0] is shown in red.

With the values of the Poisson's ratio as a function of strain along the [111] direction, we calculate the SFE for all three uniaxial strain cases. Figure 4(a) shows the dependence of the SFE dependence on strain along the [111] direction. All curves show a similar behavior. Within the strain range $0.02 < \varepsilon < 0.02$, the SFE is a nearly linear function of the [111] longitudinal strain ($d\gamma/d\varepsilon = -0.87$ J/m^2 for the simple strain case). As for the volume conserving case the SFE over the entire deformation range can be reasonably well fit by a cubic polynomial; the values of the coefficients are provided in Table II. As expected, the SFE curve for the uniaxial stress case lies between that for simple (uniaxial) strain and the volume-conserving cases. This can be easily understood since the simple strain and the volume-conserving strain cases are the two extreme cases with Poisson's ratio of 0.0 and 0.5 (for small deformation), while the Poisson's ratio of the uniaxial stress case always lies between these two.

Figure 4(b) shows the dependence of the SFE on longitudinal strain in the (111) plane of the stacking fault. The longitudinal (normal) strain was applied in four independent directions: [1$\bar{1}$0], [2$\bar{1}\bar{1}$], and two other directions with irrational Miller indices, making angles of $\pi/4$ and $3\pi/8$ with the [1$\bar{1}$0] direction, as illustrated in Fig. 1(d). In all four cases, the trends are very similar: A maximum in the SFE occurs at a (compressive) strain of approximately -0.015. The similarity in the strain dependence of the SFE at small strain is simply a result of the fact that all fcc materials are elastically isotropic in the (111) plane within the linear elastic limit (e.g., see Zhang *et al.*[41]). The SFE versus longitudinal strain in the (111) plane curves increasingly deviate as the magnitude of the strain increases simply because the linear elasticity approximation is increasingly in error at large strain.

To a reasonable approximation, all of the SFE versus longitudinal strain in the (111) plane can also be fit via a third order polynomial. The fitting coefficients are provided in Table II for all four directions.

VI. SFE OF COPPER UNDER ⟨1$\bar{1}$0⟩{111} AND ⟨11$\bar{2}$⟩{111} SHEAR STRAINS

Edge dislocations in copper tend to dissociate into Shockley partial dislocations; e.g., a dislocation with burgers vector $(a/2)[01\bar{1}]$ on a (111) glide plane may dissociate into partials with burgers vectors $(a/6)[11\bar{2}]$ and $(a/6)[\bar{1}2\bar{1}]$. These dislocations are driven by shear stresses that have components in the (111) plane along the direction parallel to the burgers vectors. Since the spacing between the partial dislocations is determined, in part, by the SFE, and because dislocation glide in Cu is driven by shear in the {111} plane, we now consider the effect of shear on the SFE itself. In particular, we consider shear strains of the form ⟨11$\bar{2}$⟩{111} and ⟨1$\bar{1}$0⟩{111}. In the former case, the crystal symmetry is such that positive and negative shear strains are inequivalent, while in the latter they are identical.

The SFE under shear strain in the ⟨1$\bar{1}$0⟩{111} directions shows little effect for strains of magnitude smaller than ∼0.04, as shown in Fig. 5(a). However, for larger strains, the SFE drops from its unstrained value of 41 to 12 mJ/m^2 at a strain of $\varepsilon = \pm 0.1$.

Figure 5(b) also shows that the SFE is nearly independent of ⟨11$\bar{2}$⟩{111} shear strain for strains of magnitude smaller than ∼0.04 (i.e., $d\gamma/d\varepsilon = 0.007$ J/m^2); there is a rapid decrease for shear strains beyond this of one sign and a much more gentle increase for shear strains of the opposite sign. We note that while the SFE is positive over the entire ⟨1$\bar{1}$0⟩{111} shear strain range considered and for one sign of the ⟨11$\bar{2}$⟩{111} shear strain, the SFE becomes negative for the other sign of ⟨11$\bar{2}$⟩{111} shear strain. As above, this indicates a stability limit for fcc Cu under shear.

VII. DISCUSSION

In order to understand the physical origin of the behavior of the SFE at large strains, we evaluate the dependence of the energy difference between the hcp and fcc phases of Cu as a function of strain. The hcp phase is identical to the fcc phase with addition of one stacking fault on every other {111} plane. Figure 6 shows the difference in energy of the fcc and hcp phases as a function of volumetric strain, and longitudinal strain along the [111] and [1$\bar{1}$0] directions. The latter direction is in the (111) plane. Similar trends are observed in the energy differences and SFE as a function of strain, shown in Figs. 2 and 4. This observation suggests that the presence of the

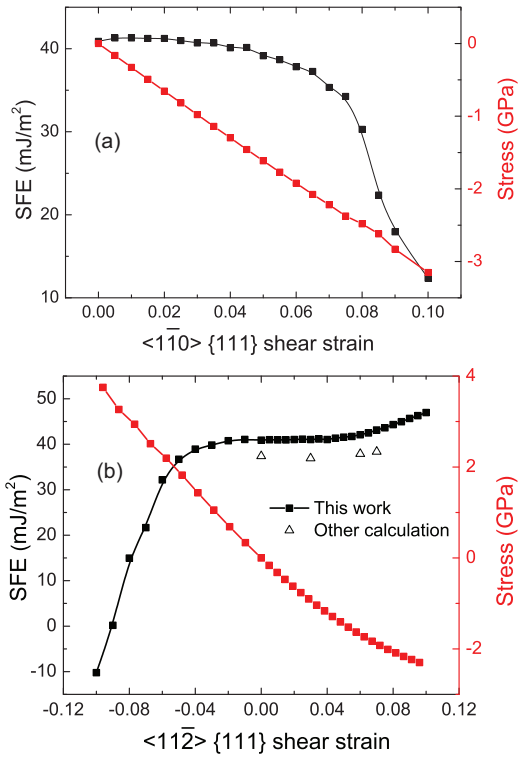

FIG. 5. (Color online) SFE curve under $\langle 1\bar{1}0\rangle\{111\}$ (a) and $\langle 11\bar{2}\rangle\{111\}$ (b) shear strains. The respective induced stress is shown in red. The calculated SFE from another theoretical study[18] is shown for comparison.

maximum in the SFE curve under longitudinal strain in the (111) plane (and its absence in the other two cases) is related to the underlying lattice thermodynamics and stability. However, the correlation with the hcp/fcc perfect crystal results is not expected to be perfect since the stacking fault is a single defect in an infinite medium, while the perfect crystal differences correspond to defects just a few atomic planes apart throughout the entire crystal.

The strain dependence of the SFE is shown to be very large at experimentally achievable strains in Cu, such as under large pressures, in high strain rate deformation, shock loading, and SPD processing. For example, the ultimate tensile strength of equal-channel angular pressing (ECAP) deformed, ultrafine grained Cu is in the order of 1 GPa.[42] At such stresses, the SFE value has changed, relative to that in the zero-strain case, by ∼50%. Such changes can have profound effects on dislocation deformation mechanisms, such as the propensity for cross slip or twinning. While it is possible that an fcc metal will undergo non-{111} slip at very large stress (activation of other "exotic" slip systems), simulations and experiments on Cu nanowires[43–46] under tensile loading have not observed such processes at stresses above 1.5 GPa.

Atomic mechanisms of deformation and damage accumulation in materials subjected to large stresses have been studied using MD simulations.[47–55] The present results indicate a strong variation of the SFE under extreme conditions of strain (stress) and suggest a revision of interatomic potentials used in these MD investigations. Widely used empirical interatomic potentials for Cu, such as those based on the EAM,[56,57] are

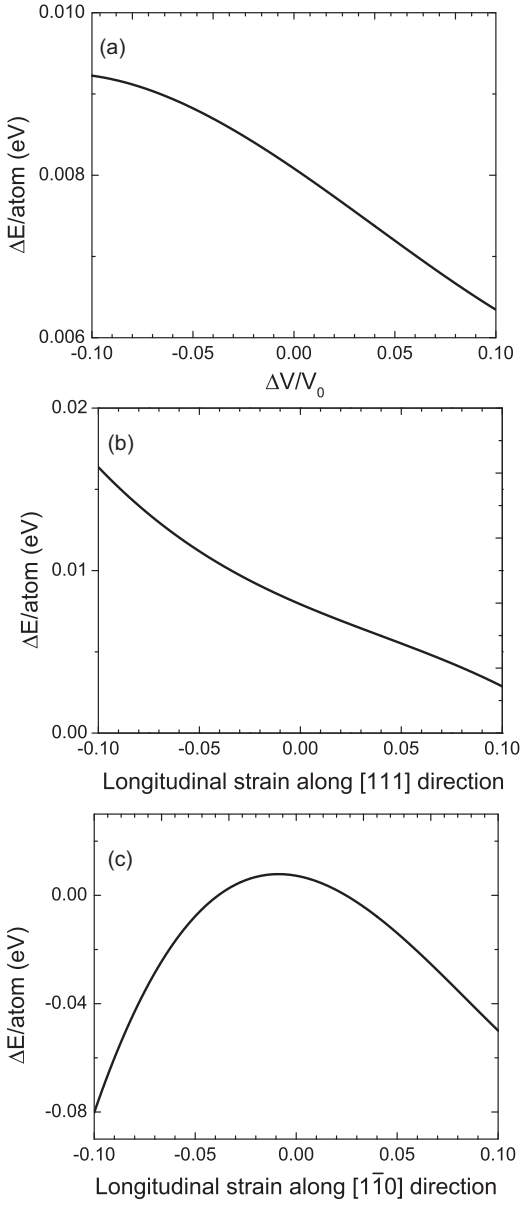

FIG. 6. Energy difference per atom for Cu in an hcp and fcc phase, $\Delta E = E(\text{hcp}) - E(\text{fcc})$, under volumetric strain (a) and longitudinal strain along (b) [111] and (c) [1$\bar{1}$0]directions.

able to capture the SFE at zero stress. In fact, such potentials are routinely fitted to this parameter. However, since they are never fitted to SFEs at large strain, it is not surprising that they do not reproduce the SFE found at large strain. An earlier study of SFE versus strain based on such empirical potentials[22] showed unphysical behavior at large strain. This suggests that use of potentials that are not able to reproduce the correct SFE versus strain could lead to unphysical results in MD simulation of high strain rate, shock, or SPD. Dislocation acceleration and motion at extreme strain rates have been modeled by MD simulations[49,52] based on an EAM potential. These simulations have shown intriguing dislocation dynamic effects, such as change in partial dislocation distance and core structure, and generation and annihilation of trailing partials. These mechanisms inherently depend on the value of the SFE. However, the potential used does not properly reproduce the

SFE with strain. As a result, the intriguing observations made, may not accurately represent the behavior of the real material. Therefore, we suggest that simulations under such high stress conditions should be performed with interatomic potentials fit to SFE versus strain data in the proper stress range, such as those found here.

As discussed above, the SFE can vary significantly with strain. SFE versus volumetric and shear strain calculations were also performed in another study.[18] We note that while the trends in this study and those found here are similar, that study showed $d\gamma/d\varepsilon|_{\varepsilon=0}$ -0.001 J/m^2, while here we find $d\gamma/d\varepsilon|_{\varepsilon=0} = -0.44$ J/m^2. In addition, a smaller discrepancy ($\sim$10%) was found for $d\gamma/d\varepsilon|_{\varepsilon=0}$ in $\langle 11\bar{2}\rangle\{111\}$ shear. We believe these discrepancies arise from the use of different convergence criteria—the convergence criteria in the present study are much more stringent (see the Appendix for convergence test results). While this led to an increase in computational cost by two orders of magnitude, such stringent convergence criteria are necessary in some cases.

VIII. CONCLUSIONS

We systematically investigated the dependence of the intrinsic stacking fault energy in copper on volumetric, longitudinal, and shear strain from small to large deformation (up to $\varepsilon = \pm 0.1$) using first-principles calculations within the density functional theory (GGA-PBE). The SFE in unstrained copper was found to be $\gamma = 41$ mJ/m^2, in reasonable agreement with the extant experimental and theoretical literature (which show a wide scatter). For volumetric (hydrostatic) strain and longitudinal strain in the direction perpendicular to the stacking fault plane, the SFE decayed monotonically with increasing (tensile) strain and increased with compressive strain. For small values of these strains, the SFE was found to be a linear function of strain (volumetric strain: $d\gamma/d\varepsilon|_{\varepsilon=0} = -0.44$ J/m^2 and longitudinal strain: $d\gamma/d\varepsilon|_{\varepsilon=0} = -0.87$ J/m^2). However, at larger strain, both SFE versus strain plots showed $d^2\gamma/d\varepsilon^2 > 0$. On the other hand, the SFE increasingly drops with increasing strain for longitudinal strain within the plane of the stacking fault; i.e., $d^2\gamma/d\varepsilon^2 < 0$. Application of shear strain parallel to the (111) intrinsic stacking fault plane has little effect on the SFE at small and moderate strain. In the $\langle 1\bar{1}0\rangle\{111\}$ shear strain case, the SFE falls rapidly with increasing strain magnitude at large strain. However, application of $\langle 11\bar{2}\rangle\{111\}$ shear strain leads to a slow rise in the SFE and a sharp drop in SFE at large strain of the opposite sign. It is interesting to note that application of large uniaxial strains perpendicular to the stacking fault plane lead to negative stacking fault energies; this represents bounds on the stability of the fcc lattice of Cu. Application of both large compressive and tensile strains in the (111) plane can also lead to a loss of stability. The trends in the variation of the SFE with volumetric and longitudinal strains are linked to the intrinsic energy differences of the fcc and hcp Cu phases. The present results suggest that care should be taken in atomistic simulations of materials at high stress based upon empirical interatomic potentials, which are usually only fitted to the zero-strain SFE. For such simulations, it is suggested that the SFE versus strain behavior should be included in the fitting of such interatomic potentials for use in high stress deformation studies.

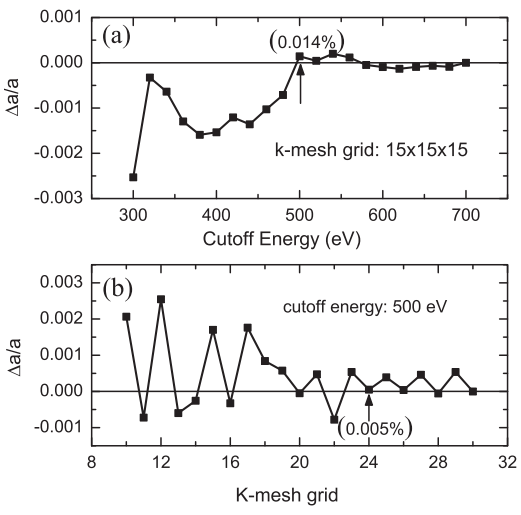

FIG. 7. Convergence of the copper lattice constant with (a) plane wave cutoff energy and (b) k-mesh grid. The reference value for the lattice constant was calculated using (a) 700 eV cutoff energy and a (b) $30 \times 30 \times 30$ k-mesh grid. The converged values chosen for the remainder of the study are indicated with the arrows along with the deviations.

ACKNOWLEDGMENTS

This work was supported by the A*STAR Computational Resource Centre through the use of its high performance computing facilities.

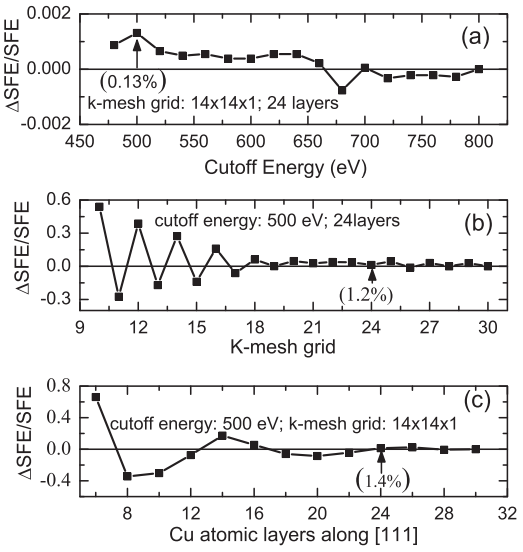

FIG. 8. Convergence of the SFE as a function of the plane wave cutoff energy, k-mesh grid, and the number of copper fcc atomic layers along the [111] direction. The reference SFE is calculated using an (a) 800 eV cutoff energy, (b) $30 \times 30 \times 1$ k-mesh grid, and (c) 30 atomic layers along the [111] direction, respectively. The converged values used in the work are indicated by the arrows along with the deviations in the SFE.

APPENDIX: DFT CONVERGENCE TESTS—LATTICE PARAMETER AND SFE VERSUS CUTOFF ENERGY, *k*-MESH GRID, AND NUMBER OF ATOMIC LAYERS

As discussed in the text, the values of the SFE under strain are very sensitive to the convergence criteria adopted in the calculations. This can be traced to how the SFE is calculated; using energy differences between a perfect reference system and a system with a single stacking fault. Since the energy differences are in the range of meV, accurate SFE results require very accurate calculations in each system. We therefore used strict criteria of the convergence of the calculations carefully choosing the values of the cutoff energy, *k*-mesh grid, and the number of fcc atomic layers employed in the calculations.

The equilibrium lattice parameter is obtained by full relaxation of the atomic coordinates and the lattice constants by minimizing the stress tensor and the atomic forces (with appropriate boundary conditions). During optimization of the copper unit cell in VASP, we restarted the calculations several times in order to achieve strict convergence of the lattice parameter minimizing the error coming from the constant basis set used. We plotted the lattice constant as a function of the cutoff energy and *k*-mesh grid in Fig. 7. The deviation of the lattice constant is calculated relative to the perfect crystal reference calculated with the largest cutoff energy, 700 eV, and the largest *k*-mesh grid, 30 × 30 × 30, respectively. The lattice constant deviation for 500 eV is only 0.014% as shown in Fig. 7(a), using a *k*-mesh grid 15 × 15 × 15. The lattice constant deviation for the *k*-mesh grid 24 × 24 × 24 is 0.005% as shown in Fig. 7(b), using a cutoff energy of 500 eV.

With the convergence parameters obtained from the lattice parameter optimization, we tested the convergence of the SFE for the actual supercells used in the investigation. The variation of the SFE displayed in Fig. 8 is evaluated with respect to the reference value calculated with the largest cutoff energy, 800 eV, the largest number of *k*-mesh grid, 30 × 30 × 1, and the largest atomic layers along the [111] direction, 30, respectively. From the convergence tests the final values of cutoff energy, *k*-mesh grid, and atomic layers chosen and their deviations were 500 eV (0.13%), 24 × 24 × 1 (1.2%), and 24 layers (1.4%). The fixed *k*-mesh grid, number of atomic layers, and energy cutoff used in the tests (two fixed at a time) is 14 × 14 × 1, 24, and 500 eV, respectively.

*branicio@ihpc.a-star.edu.sg

[1] P. C. J. Gallagher and Y. C. Liu, Acta Metall. **17**, 127 (1969).
[2] C. W. Lung and N. H. March, *Mechanical Properties of Metals: Atomistic and Fractal Continuum Approaches* (World Scientific, Singapore, 1999).
[3] F. Ebrahimi, Z. Ahmed, and H. Li, Appl. Phys. Lett. **85**, 3749 (2004).
[4] Y. H. Zhao, Y. T. Zhu, X. Z. Liao, Z. Horita, and T. G. Langdon, Appl. Phys. Lett. **89**, 121906 (2006).
[5] W. D. Callister, *Materials Science and Engineering: An Introduction* (Wiley, New York, 2007).
[6] A. D. Rollett, *Materials Processing and Texture*, edited by A. D. Rollett (Wiley, New York, 2008).
[7] P. Gallagher, Metall. Mater. Trans. B **1**, 2429 (1970).
[8] A. Howie and P. R. Swann, Philos. Mag. **6**, 1215 (1961).
[9] L. E. Murr, Phys. Status Solidi A **3**, 447 (1970).
[10] D. Heidenreich and W. Shockley, *Report on a Conference on Strength of Solids* (The Physical Society, London, 1948), p. 57.
[11] R. L. Fullman, J. Appl. Phys. **22**, 448 (1951).
[12] H. Suzuki, in *Yamanda Conference IX on Dislocations in Solid*, edited by H. Suzuki, T. Ninomiya, K. Sumino, and S. Takeuchi (Tokyo University Press, Tokyo, Japan, 1984).
[13] S. Qu, X. H. An, H. J. Yang, C. X. Huang, G. Yang, Q. S. Zang, Z. G. Wang, S. D. Wu, and Z. F. Zhang, Acta Mater. **57**, 1586 (2009).
[14] T. C. Schulthess, P. E. A. Turchi, A. Gonis, and T. G. Nieh, Acta Mater. **46**, 2215 (1998).
[15] N. R. Tao and K. Lu, Scr. Mater. **60**, 1039 (2009).
[16] V. S. Sarma, J. Wang, W. W. Jian, A. Kauffmann, H. Conrad, J. Freudenberger, and Y. T. Zhu, Mater. Sci. Eng. A **527**, 7624 (2010).
[17] M. H. Jhon, A. M. Glaeser, and D. C. Chrzan, Phys. Rev. B **71**, 214101 (2005).
[18] C. Brandl, P. M. Derlet, and H. Van Swygenhoven, Phys. Rev. B **76**, 054124 (2007).
[19] R. M. J. Cotteril and M. Doyama, Phys. Rev. **145**, 465 (1966).
[20] S. Schweizer, C. Elsasser, K. Hummler, and M. Fahnle, Phys. Rev. B **46**, 14270 (1992).
[21] N. M. Rosengaard and H. L. Skriver, Phys. Rev. B **47**, 12865 (1993).
[22] P. Heino, L. Perondi, K. Kaski, and E. Ristolainen, Phys. Rev. B **60**, 14625 (1999).
[23] S. Ogata, J. Li, and S. Yip, Science **298**, 807 (2002).
[24] Y. Qi and R. K. Mishra, Phys. Rev. B **75**, 224105 (2007).
[25] V. E. Peissker, Acta Metall. **13**, 419 (1965).
[26] W. M. Stobbs and C. H. Sworn, Philos. Mag. **24**, 1365 (1971).
[27] P. E. Blochl, Phys. Rev. B **50**, 17953 (1994).
[28] J. Hafner, J. Comput. Chem. **29**, 2044 (2008).
[29] J. P. Perdew, K. Burke, and M. Ernzerhof, Phys. Rev. Lett. **77**, 3865 (1996).
[30] M. Methfessel and A. T. Paxton, Phys. Rev. B **40**, 3616 (1989).
[31] C. Bercegeay and S. Bernard, Phys. Rev. B **72**, 214101 (2005).
[32] H. J. Monkhorst and J. D. Pack, Phys. Rev. B **13**, 5188 (1976).
[33] I.-K. Suh, H. Ohta, and Y. Waseda, J. Mater. Sci. **23**, 757 (1988).
[34] J. P. Hirth and J. Lothe, *Theory of Dislocations* (Wiley, New York, 1982).
[35] A. F. Bower, *Applied Mechanics of Solids* (CRC Press, Boca Raton, FL, 2011).
[36] J. F. Nye, *Physical Properties of Crystals* (Clarendon Press, Oxford, 1957).
[37] A. Ballato, IEEE Trans. Ultrason. Ferroelectr. Freq. Control **43**, 56 (1996).
[38] G. R. Johnson and W. H. Cook, Eng. Fract. Mech. **21**, 31 (1985).
[39] W. C. Overton, Jr. and J. Gaffney, Phys. Rev. **98**, 969 (1955).
[40] H. Wang and M. Li, Phys. Rev. B **79**, 224102 (2009).
[41] J.-M. Zhang, Y. Zhang, K.-W. Xu, and V. Ji, J. Phys. Chem. Solids **68**, 503 (2007).

[42]Y.-H. Zhao, J. F. Bingert, X.-Z. Liao, B.-Z. Cui, K. Han, A. V. Sergueeva, A. K. Mukherjee, R. Z. Valiev, T. G. Langdon, and Y. T. Zhu, Adv. Mater. **18**, 2949 (2006).
[43]Z. X. Wu, Y. W. Zhang, M. H. Jhon, J. R. Greer, and D. J. Srolovitz, Acta Mater. **61**, 1831 (2013).
[44]D. C. Jang, X. Y. Li, H. J. Gao, and J. R. Greer, Nat. Nanotechnol. **7**, 594 (2012).
[45]A. T. Jennings, J. Li, and J. R. Greer, Acta Mater. **59**, 5627 (2011).
[46]D. C. Jang, C. Cai, and J. R. Greer, Nano Lett. **11**, 1743 (2011).
[47]P. S. Branicio and J. P. Rino, Phys. Rev. B **62**, 16950 (2000).
[48]P. S. Branicio, R. K. Kalia, A. Nakano, and P. Vashishta, Phys. Rev. Lett. **96**, 065502 (2006).
[49]H. Tsuzuki, P. S. Branicio, and J. P. Rino, Appl. Phys. Lett. **92**, 191909 (2008).
[50]P. S. Branicio, R. K. Kalia, A. Nakano, P. Vashishta, F. Shimojo, and J. P. Rino, J. Mech. Phys. Solids **56**, 1955 (2008).
[51]C. Zhang, R. K. Kalia, A. Nakano, P. Vashishta, and P. S. Branicio, J. Appl. Phys. **103**, 083508 (2008).
[52]H. Tsuzuki, P. S. Branicio, and J. P. Rino, Acta Mater. **57**, 1843 (2009).
[53]P. S. Branicio, R. K. Kalia, A. Nakano, and P. Vashishta, Appl. Phys. Lett. **97**, 111903 (2010).
[54]H. Tsuzuki, J. P. Rino, and P. S. Branicio, J. Phys. D: Appl. Phys. **44**, 055405 (2011).
[55]P. S. Branicio, J. Comput. Theor. Nanosci. **9**, 1870 (2012).
[56]M. S. Daw, S. M. Foiles, and M. I. Baskes, Mater. Sci. Rep. **9**, 251 (1993).
[57]Y. Mishin, M. J. Mehl, D. A. Papaconstantopoulos, A. F. Voter, and J. D. Kress, Phys. Rev. B **63**, 224106 (2001).